Laser-assisted radiative recombination in a cold hydrogen plasma

I. I. Fabrikant, H. B. Ambalampitiya

Department of Physics and Astronomy,

University of Nebraska, Lincoln, Nebraska 68588-0299, USA

(Dated: August 12, 2024)

Abstract

We study the process of laser-assisted radiative recombination of an electron with a proton in a cold hydrogen plasma employing the semiclassical Kramers' approach which involves calculation of classical trajectories in combined laser and Coulomb fields and the use of the correspondence principle. Due to the Coulomb focusing effect, recombination is the most effective when the initial electron momentum is parallel to the laser polarization. Orders of magnitude enhancement of the cross section, as compared to the laser-free case, is observed in this case. With increasing angle between the electron momentum and polarization, the recombination cross section drops. However, even after averaging over Maxwellian velocity distribution we obtain a substantial enhancement of the recombination rate constant, as compared to the zero-field case. For the field intensities in the range 30-350 MW/cm^2, the enhancement occurs in the region of the radiation wavelength from 5 to 20 μm and for the plasma temperature from 20 to 300 K.

I. INTRODUCTION

The processes of low-energy laser-assisted few-body collisions and reactions have been explored in several recent works [1–3]. In the present paper we investigate the laser-assisted radiative recombination (LARR) process

$$e^- + A^{+(n)} + n\hbar\omega \to A^{+(n-1)} + n'\hbar\omega + \hbar\Omega$$

which at high intensities (occupation numbers n and n' are large) can be treated as a spontaneous radiative recombination in the presence of a classical field of frequency ω. It is a nonresonant process since the frequency of the laser field ω is not equal to the emitted photon frequency Ω which is typically much greater than ω.

The LARR is the final step of the high-order harmonic generation process (HHG) [4–6] when electron is captured by an ion by emitting high-frequency photon in an infrared field. The LARR process could be also of interest for antihydrogen studies [7], particular for the ALPHA collaboration studies where a similar charge-conjugated process

$$e^+ + \bar{p} \to \bar{\mathrm{H}} + \hbar\Omega$$

is one of the main mechanisms of the antihydrogen formation [8–13], the other being three-body recombination

$$\bar{p} + e^+ + e^+ \to \bar{\mathrm{H}} + e^+.$$

The two reactions have very different dependencies on the temperature of the positron cloud or plasma and on the positron density [9, 11, 13, 14], and produce very different antihydrogen states. Whereas the three-body recombination tends to produce highly excited states of $\bar{\mathrm{H}}$, the radiative recombination results in formation of mostly ground state. Studies which have been conducted so far indicate that RR plays some role in these conditions, but, as far as we are aware, there is no quantitative estimates of the relative significance of RR. However, if its contribution is small, laser-assisted process can enhance it, particularly for electron capture into the ground and low-excited states since the three-body process is dominated by capture into highly-excited states. Therefore studies of both reactions are of paramount importance for understanding of antihydrogen formation.

In our two previous papers [15, 16] we have shown that for low enough electron energies the radiative recombination and related bremsstrahlung process can be strongly enhanced

by infrared laser radiation in the range of intensities between 1 GW/cm^2 and 1 TW/cm^2 due to the Coulomb focusing effect. The direction of the electron velocity chosen in these calculation was parallel to the field polarization. Intuitively it is clear that for this geometry the enhancement is most efficient. However, in experimental conditions of storage rings [17–21] the electron beam has a component perpendicular to the polarization vector. Moreover, in antihydrogen studies [7, 8, 11, 13] the trapped positron-antiproton clouds form a plasma, therefore for calculation of the reaction rate, the rate constant should be averaged over the Maxwellian velocity distribution.

In the present paper we consider electron-proton (or positron-antiproton) plasma in a trap at the temperatures varying from 10 to 300 K. To be specific, we will be discussing electron-proton recombination, but the same conclusion will be applicable to the charge-conjugated process. It is well known that the spontaneous radiative recombination process in this case

$$e + p \to \mathrm{H} + \hbar\Omega$$

has a rather low rate, therefore we explore the possibility to enhance it by placing the system in an infrared field. The idea to use the resonance process of laser-stimulated recombination for antihydrogen formation was explored in [17–23]. In contrast we use a nonresonant field frequency which is much lower than the frequency of radiated photon, and lies in the infrared or far infrared region. One of the advantages of this approach is that the reionization process is suppressed unless the field intensity is high enough to induce the tunneling ionization. Therefore in the present studies we employ a relatively weak field with intensity less than 350 MW/cm^2 for which multiphoton or tunneling ionization from the ground or low-excited states is negligible [16].

The ratio of the laser-assisted recombination cross section to the zero-field cross section, or the gain factor, is strongly dependent on the parameter [16]

$$\chi = \frac{\omega v_0}{F_0}, \tag{1}$$

where v_0 is the electron velocity before entering the laser field region, and F_0 is the electric field amplitude. (Atomic units are used throughout the paper.) To understand the physical significance of this parameter, consider one-dimensional electron motion in a pure laser field

$$F = F_0 \cos(\omega t + \phi_0)$$

with the mean velocity

$$\bar{v} = v_0 - \frac{F_0}{\omega}$$

where $v_0 > 0$ is the speed at $t = 0$. The electron will approach the target if $\bar{v} > 0$, i.e., $0 < \phi_0 < \phi_1$ or $\pi - \phi_1 < \phi_0 < 2\pi$ where $\phi_1 = \arcsin\chi$ where χ is given by Eq. (1). In the range of ϕ_0 the probability is nonzero, and it peaks at values of ϕ_0 close to ϕ_1 or $\pi - \phi_1$. Therefore the gain factor is large for $\chi \leq 1$ or χ slightly exceeding 1. After going through maximum in the vicinity of $\chi = 1$ it drops sharply. The physical reason for this is that at low $\bar{v}$ a strong Coulomb focusing [15, 16] occurs which makes the electron to approach very close to the proton even for large impact parameters. Since the efficient radiation occurs only at very close distances between charged particles, the Coulomb focusing effect leads to a strong enhancement of radiation in both bremsstrahlung and radiative recombination processes. For a typical electron velocity in a 20 K electron-proton plasma and the infrared radiation with frequency $\omega = 0.0043$ a.u. ($\lambda = 10.6\mu$m) this implies that the laser intensity should be higher than 100 MW/cm^2. By further increasing the wavelength we can achieve efficient recombination even for lower laser intensity. In the present paper we explore the infrared field in the intensity range between 14 and 350 MW/cm^2 and the frequency range between 0.001 and 0.007 a.u. (wavelength between 45 and 6.5 μm). In the following we will be using atomic units, unless stated otherwise.

II. THEORY

Our theory [16] is based on the semiclassical approach of Kramers [24] developed even before the creation of quantum mechanics. It uses the classical theory of radiation and the Bohr's correspondence principle. In the absence of the external field, the Kramers' formula works very well even for the capture into the ground state, and we assume the same accuracy in the presence of the field. We will start with outlining the Kramers' aproach for the zero field [16]. Suppose an electron collides with a Coulomb center of charge Z. Since most of the radiation occurs when the electron is close to the center, we assume motion along a parabolic orbit with eccentricity ϵ close to 1. Then, using the classical theory of radiation [25], we obtain for the power radiated

$$I_s = \frac{64 \cdot 2^{2/3} s^{4/3} \mathcal{E}^4}{3c^3 Z^2} \left\{ (1-\epsilon^2)\mathrm{Ai}^2(u) + \left(\frac{2}{s}\right)^{2/3} (\mathrm{Ai}')^2(u) \right\} \tag{2}$$

where s is the harmonics order, $s = \omega T/2\pi$, ω is the frequency of the emitted radiation, and T is the period of revolution of the electron on the orbit, $\mathcal{E}$ is the electron energy on the orbit, and

$$u = \left(\frac{s}{2}\right)^{2/3}(1-\epsilon^2).$$

Using the Bohr's correspondence principle [16], we obtain for the probability P_n of emission of a photon for a given electron angular momentum l accompanied by electron capture into the state with the principal quantum number n

$$P_n = \frac{8\pi \cdot 2^{4/3}}{3c^3 n^3 \Omega_n^{1/3}}[(\mathrm{Ai}')^2(u) + u\mathrm{Ai}^2(u)], \quad u = \left(\frac{\Omega_n}{2}\right)^{2/3} l^2, \tag{3}$$

where the classical orbital angular momentum l is related to the impact parameter b as $l = (2E)^{1/2}b$, and Ai is the Airy function. Summing over all l we obtain theKramers' result for the radiative recombination cross section

$$\sigma_n(E) = \frac{\beta_n}{(E+\epsilon_n)E},$$

where E is the initial electron energy, ϵ_n is the absolute value of the energy of the final (bound) state, so that the frequency of the emitted photon $\Omega_n = E + \epsilon_n$, and

$$\beta_n = \frac{8\pi}{3\sqrt{3}c^3 n^3},$$

where $c = 137.04$ a.u. is the speed of light, and n is the principal quantum number of the final hydrogen state. The corresponding recombination rate constant is

$$\alpha_n(T) = \int \sigma_n(E)(2E)^{1/2} f(T,E) dE,$$

where $f(T,E)$ is the Maxwellian distribution function

$$f(T,E) = \frac{2E^{1/2}}{\pi^{1/2}T^{3/2}} e^{-E/T},$$

and T is the temperature in energy units.

The integration results in

$$\alpha_n(T) = \frac{\beta_n}{\pi^{1/2}} \left(\frac{2}{T}\right)^{3/2} e^{\epsilon_n/T} E_1\left(\frac{\epsilon_n}{T}\right),$$

where $E_1(x)$ is the exponential integral. Since in our case $\epsilon_n \gg T$, we can use the asymptotic expression for E_1 with the result

$$\alpha_n(T) = \frac{2^{3/2}\beta_n}{(\pi T)^{1/2}\epsilon_n}.$$

To extract the explicit dependence on the principal quantum number n, we use

$$\beta_n = \beta_0 \epsilon_n^{3/2}, \quad \beta_0 = \frac{16\pi\sqrt{2}}{3\sqrt{3}c^3}, \quad \epsilon_n = \frac{1}{2n^2}.$$

Then

$$\alpha_n(T) = \frac{2\beta_0}{(\pi T)^{1/2} n}. \tag{4}$$

For a temperature $T = 20$ K and $n = 1$ we get $\alpha_1 = 0.553 \times 10^{-3}$ a.u.$=3.39 \times 10^{-12}$ cm^3/s, and $\alpha_1(T)$ decreases with the growth of T and n according to (4). Bell and Bell [26] obtained analytical expressions for the cross section summed over all n, but the process is dominated by $n = 1$, in contrast to the three-body recombination dominated by capture into states with high n [14].

Switching now to LARR, we consider the electron motion in the electric field (linearly polarized along the z axis)

$$F(t) = F_0 \cos(\omega t + \phi_0). \tag{5}$$

The theory developed in [16] was restricted to the case when the incident electron velocity is parallel to the electric-field polarization vector, therefore it should be modified to account for a general geometry.

In the presence of the laser field we integrate numerically the classical trajectory with the initial impact parameter vector $\mathbf{b}$ until electron approaches close enough to the Coulomb center (proton) where it acquires angular momentum $l_{\min}(\mathbf{b})$. The distance of the closest approach and $l_{\min}$ also depend on the orientation of the initial velocity $\mathbf{v}$ relative to the field vector $\mathbf{F}$. In the vicinity of the Coulomb center the laser field can be neglected, and the radiation probability is calculated according to Eq. (3) with $l = l_{\min}$.

Since the radiation probability is substantial only when the electron is close to the proton, it is of paramount importance to take into account the full electron-proton interaction including the Coulomb singularity, without its softening. It is well known that the numerical solutions for the equations of motion near the Coulomb center become highly unstable due to this singularity. This problem is solved by the regularization of Coulomb trajectories based on the formalism of extended Hamiltonian [27]. This method was previously developed and applied to the process of bremsstrahlung in the Coulomb field [15]. A similar method was applied to the strong-field ionization of H_2 [28] and classical treatment of the electron-impact ionization problem [29, 30].

Let us introduce two coordinate systems: unprimed with the z axis along $\mathbf{F}$, and primed with the z' axis along $\mathbf{v}$ as shown in Fig. 1. The orientation of $\mathbf{v}$ in the unprimed system is characterized by angles θ_v and ϕ_v By choosing y' axis in the xy plane, we have for the Cartesian coordinates of the base primed vectors

$$\hat{x'} = (\cos\theta_v \cos\phi_v, \cos\theta_v \sin\phi_v, -\sin\theta_v), \tag{6}$$

$$\hat{y'} = (-\sin\phi_v, \cos\phi_v, 0), \tag{7}$$

$$\hat{z'} = (\sin\theta_v \cos\phi_v, \sin\theta_v \sin\phi_v, \cos\theta_v). \tag{8}$$

We start a trajectory with the following initial conditions in the cylindrical coordinates (ρ', z', ϕ')

$$\rho' = b, \quad z' = -d, \quad \phi' = \phi'_i,$$

$$\dot{z}' = v, \quad \dot{\rho}' = \dot{\phi}' = 0,$$

where b is the impact parameter, and d is a large distance such that the Coulomb interaction can be neglected as compared to the interaction with the laser field. Trajectory calculations are done more conveniently in the unprimed system where the initial conditions are given by the transformation (see Fig. 1 and Appendix A)

$$z = -d\cos\theta_v - b\cos\phi'\sin\theta_v,$$

$$x = -d\sin\theta_v\cos\phi_v + b\cos\phi'\cos\theta_v\cos\phi_v - b\sin\phi'\sin\phi_v,$$

$$y = b\sin\phi'\cos\phi_v + b\cos\phi'\cos\theta_v\sin\phi_v - d\sin\theta_v\sin\phi_v.$$

We calculate then the initial unprimed cylindrical coordinates as

$$\rho = (x^2 + y^2)^{1/2}, \quad \phi = \arctan\frac{y}{x}, \tag{9}$$

$$\dot{\rho} = \frac{xv_x + yv_y}{\rho}, \quad \dot{z} = v_z, \quad \dot{\phi} = \frac{xv_y - v_x y}{\rho^2}, \tag{10}$$

where $v_x = v\sin\theta_v\cos\phi_v$, $v_y = v\sin\theta_v\sin\phi_v$, $v_z = v\cos\theta_v$.

The cross section for a fixed velocity orientation is given by

$$\sigma_n(\theta_v, \phi_v, \phi_0) = \int_0^\infty dbb \int_0^{2\pi} d\phi' P_n(b, \phi', v, \theta_v, \phi_v, \phi_0).$$

Integration over ϕ' makes the result cylindrically symmetric, therefore σ_n is independent of ϕ_v, and the integral can be calculated for any value of ϕ_v. The probability depends on

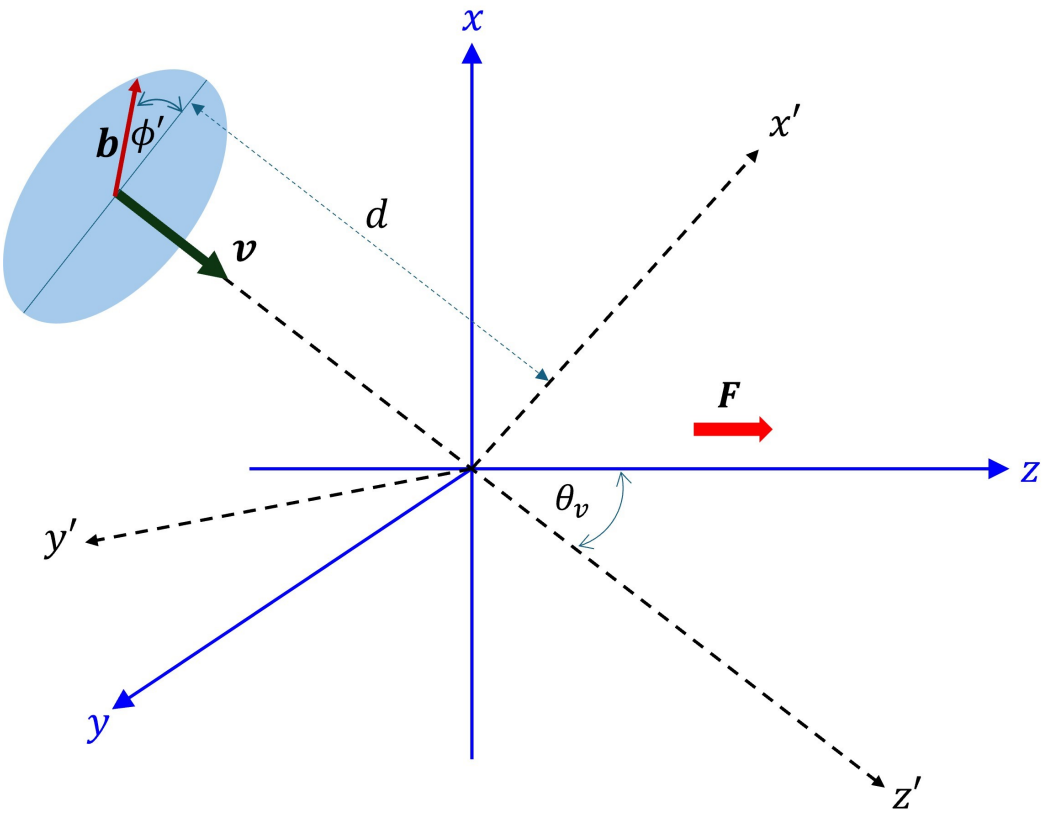

FIG. 1. Geometry of the problem. The initial velocity $\mathbf{v}$ is directed along the z' axis whose orientation in the unprimed system is given by the spherical angles θ_v and ϕ_v. The impact parameter vector $\mathbf{b}$ lies in the plane parallel to the $x'y'$ plane. Its orientation in this plane characterized by the angle ϕ'. y' axis is chosen to lie in the xy plane.

the phase ϕ_0 entering Eq. (5) for the electric field, and should be averaged over it. This is equivalent to averaging over the electron position when it enters the field region:

$$\bar{\sigma}_n(\theta_v) = \frac{1}{2\pi}\int_0^{2\pi} d\phi_0 \int_0^{\infty} dbb \int_0^{2\pi} d\phi' P_n(b, \phi', v, \theta_v, \phi_v, \phi_0). \tag{11}$$

The averaged cross section is apparently symmetric with respect to transformation $\theta_v \to \pi - \theta_v$, therefore θ_v integration can be carried out from 0 to $\pi/2$ with subsequent multiplication by 2.

For plasma applications we have to calculate the rate constant averaged over all orientations of the velocity vector $\mathbf{v}$, and also over the Maxwellian distribution in v:

$$\alpha_n(T) = \int_0^{2\pi} d\phi_0 \int_0^{\infty} dv f(T, v) v \int_0^{\infty} dbb \int_0^{2\pi} d\phi' \int_0^{\pi} d\theta_v \sin\theta_v P_n(b, \phi', v, \theta_v, \phi_v, \phi_0), \tag{12}$$

where

$$f(T,v) = (2\pi T)^{-3/2} v^2 \exp(-v^2/2T)$$

is the normalized Maxwellian distribution, and the extra 2π factor in (12) is due to integration over ϕ_v.

Integrals (11) and (12) are calculated by the Monte Carlo (MC) method with the number of points in the integrand varied from 2×10^5 to 10^6 to achieve convergence. Since classical scattering in combined fields is chaotic [31–33], the emission probability is a random function of the impact parameter and the constant phase of the laser field [16]. This feature increases the statistical uncertainty in calculation of integrals which was estimated by standard methods. In addition, a very large range of impact parameters is contributing to the integral. In this situation an efficient integration can be achieved by partitioning the whole range of b into several segments (5 to 10) and performing MC integration in each segment. For θ_v close to 0 or π, because of the Coulomb focusing effect, the range of b contributing to the LARR cross section is infinite, and the cross section is infinite accordingly [16]. To make the cross section and the rate constant finite, we make the duration of the laser pulse t_p finite, in the 5 ps - 20 ps range. In this case the trajectories corresponding to impact parameter higher than $b_{\max}(t_p)$ do not have enough time to reach the Coulomb center. Calculations show that for θ_v close to 0 convergent results can be obtained with $\rho_{\max} = 4200$ a.u. if $t_p = 5$ ps, and with $\rho_{\max} = 7000$ a.u. if $t_p = 25$ ps. However, the rate constant, Eq. (12), is convergent even when $t_p \to \infty$ because contribution of θ_v close to 0 is suppressed due to the factor $\sin\theta_v$ in the integrand. Another factor limiting the cross section is the plasma screening effect which makes the effective cut-off of the Coulomb interaction at distances of the order of the Debye screening length. A typical Debye screening length in the antihydrogen plasma is about 10-100 μm [7], or about $10^5 - 10^6$ a.u. Although it is large on the microscopic scale, it can still play a role as a limiting factor making the LARR cross section finite. Also, in other plasma applications, the effect of screening might be more significant.

III. RESULTS AND DISCUSSION

All results presented below are for recombination into the ground state since this branch is dominant. In Fig. 2 we present the LARR cross section as a function of the angle θ_v, Eq. (11), for four values of the electron velocity. The general trend is clear: cross section

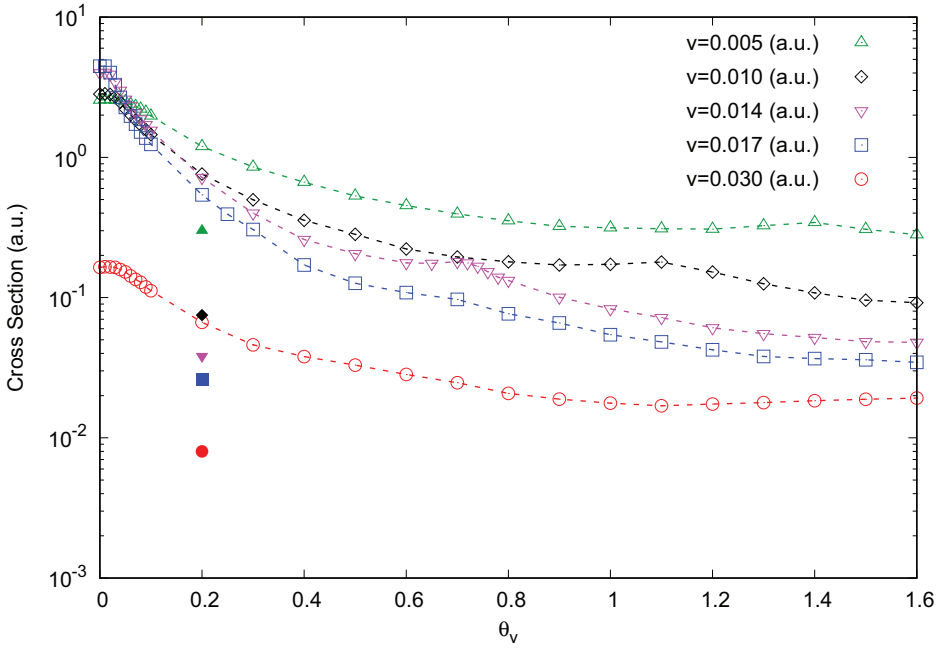

FIG. 2. LARR cross section as a function of the incident angle θ_v averaged over the initial phase ϕ_0 for selected values of electron velocity v, field amplitude $F_0 = 0.2 \times 10^{-4}$, field frequency $\omega = 10^{-3}$ a.u., except the case $v = 0.014$ when $F_0 = 0.6 \times 10^{-4}$ a.u., $\omega = 3.5 \times 10^{-3}$ a.u. The calculated values are represented by open symbols, and are joined by dashed lines for a better view. Zero-field cross sections are marked by corresponding full symbols at the left side of the graph. They are independent of θ_v.

achieves maximum when $\mathbf{F}$ is parallel to the initial velocity $\mathbf{v}$, and goes through minimum when θ_v is close to $\pi/2$. For some values of the field parameters there is a shallow maximum in the region between $\theta_v = 0.7$ and 1.1 rad. The cross section is symmetric with respect to the transformation $\theta_v \to \pi - \theta_v$. The enhancement (gain factor) is very large for θ_v close to 0, but drops substantially when θ_v approaches $\pi/2$ becoming close to 1.

To understand this behavior, in Fig. 3 we present typical trajectories for $\theta_v = 0$, $\pi/6$, $\pi/4$, and $\pi/2$. The chosen parameters are $v = 0.017$ a.u., $F_0 = 0.6 \times 10^{-4}$ a.u., $\omega = 10^{-3}$ a.u., impact parameter $b = 50$ a.u., $\phi' = 1$ rad, $\phi_0 = 1$ rad, $\phi_v = 1.28$ rad. Each trajectory represents a class of trajectories with the same angle of incidence but different

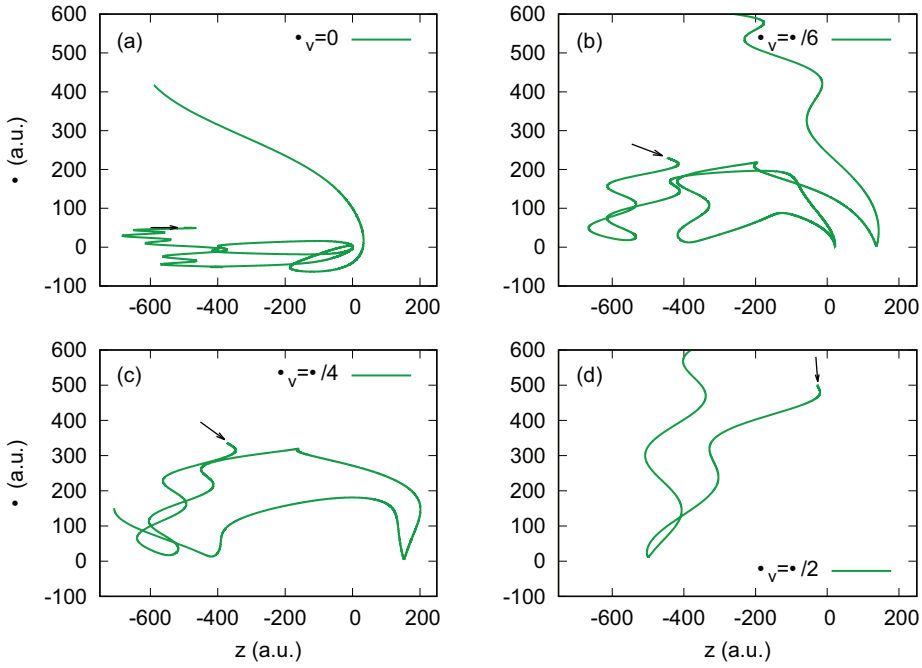

FIG. 3. Electron trajectory in the $z-\rho$ plane in the field $F = 0.6 \times 10^{-4}$ for the initial electron velocity making angle θ_v with the field polarization vector, impact parameter $b = 50$ a.u. The proton is placed at the origin of the coordinate system $(\rho, z) = (0, 0)$. The arrows indicate the launching points for each trajectory. See the text regarding the negative values of ρ.

impact parameters. Due to the chaotic dependence of the radiation probability on the impact parameter not all trajectories from this class lead to radiation. The contribution of "successful" trajectories to the total LARR cross section can be seen from Fig. 2 of Ref. [16]. The Coulomb focusing effect is mostly pronounced at $\theta_v = 0$, and it occurs in a very broad range of impact parameters as long as parameter χ, Eq. (1), is less or close to 1 [15, 16]. In this case the electron performs several oscillations due to the laser field which allows a longer action of the Coulomb field pulling the electron to its site. In contrast, in the absence of the laser field, for large impact parameters, the electron moves along almost rectilinear trajectory with virtually no displacement towards the Coulomb center.

For $\theta_v = 0$ the trajectory is planar corresponding to a fixed polar angle ϕ. However, for $\theta_v > 0$ trajectories become three-dimensional, and we show their projection on the $\rho - z$

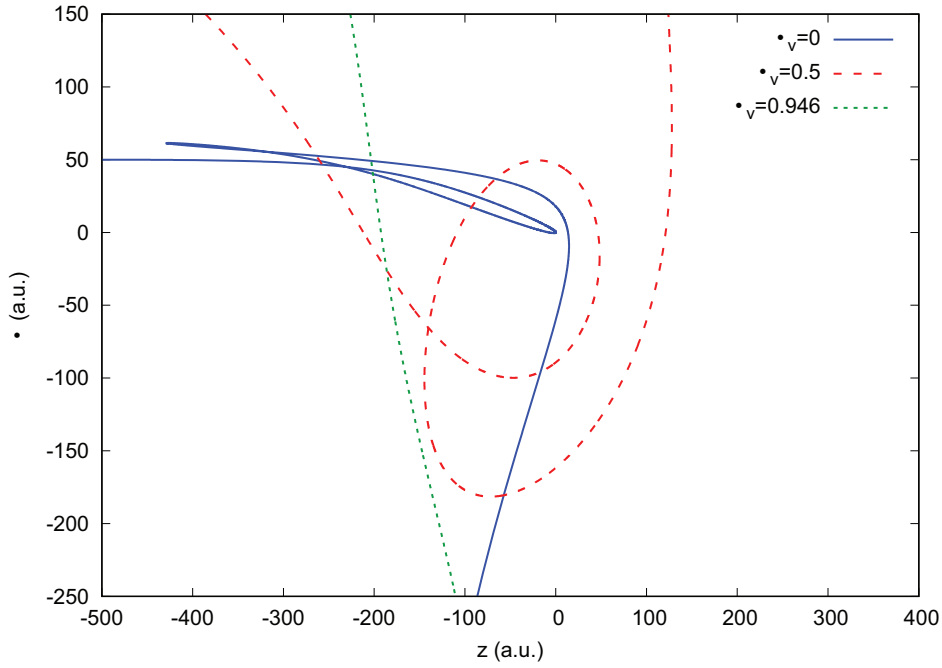

FIG. 4. A sample of planar trajectories for $F = 0.2 \times 10^{-4}$ a.u., $v = 0.1$ a.u., $\omega = 0.2 \times 10^{-3}$ a.u., $b = 50$ a.u., $\phi' = 0$, $\phi_0 = 2.5$, $\phi_v = 1.28$ and different values of the angle θ_v.

plane. Note that when the trajectory is planar, the polar angle ϕ is constant, and the trajectory can cross the z axis corresponding to a sudden change of the polar angle from ϕ to $\phi + \pi$. It is more convenient to represent this change by changing the sign of the polar coordinate ρ. In particular the first trajectory in Fig. 3 is a planar trajectory involving negative values of ρ. In this case the vector of the initial velocity $\mathbf{v}$ is parallel to the field polarization vector, but there are more cases of planar trajectories discussed in Appendix B. A sample of this kind of trajectories for three values of θ_v is presented in Fig. 4 for $b = 50$ a.u., $\phi' = 0$, $\phi_0 = 2.5$ and $\phi_v = 1.28$. In all figures the same pattern is observed: with the increase of θ_v the probability for electron to hit the proton is decreasing. It is apparent that the Coulomb focusing is most efficient for θ_v close to 0. With increasing θ_v large impact parameters do not lead to close approach, similar to the case $F_0 = 0$.

In Figs. 5 and 6 we present the ratio of the laser-assisted recombination rate constant to the zero-field rate constant (the gain factor) as a function of the field frequency ω for several

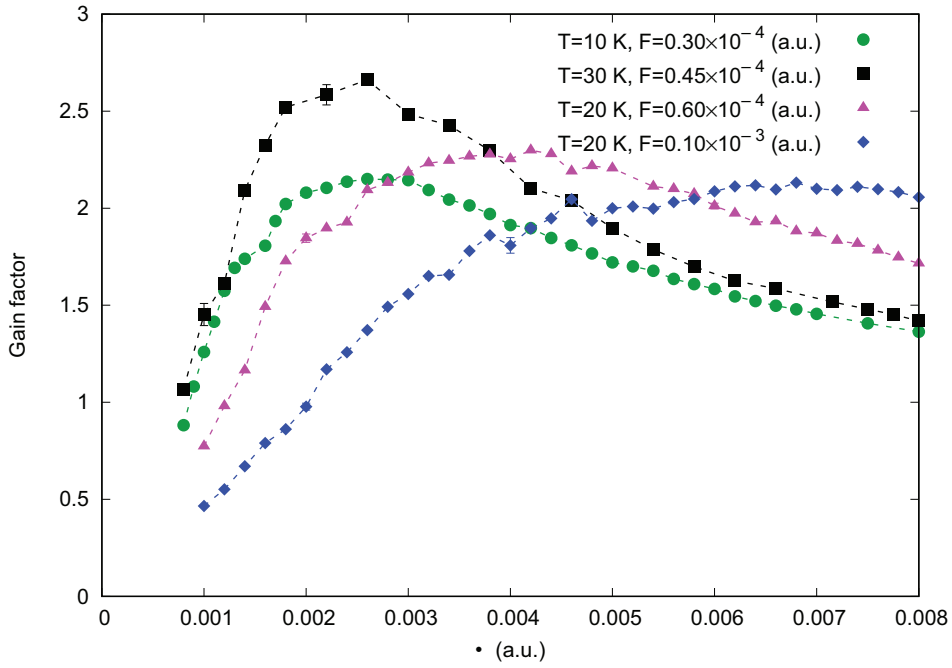

FIG. 5. The ratio of the RR rate constant for laser-assisted recombination to the zero-field rate as a function of laser frequency for several values of the field strength and low electron temperatures. Typical error bars are shown for selected points.

selected values of field intensities and temperatures. Uncertainties of the results are partly due to the chaotic dependence of the radiation probability on the impact parameter [16, 31], and partly due to the MC integration error. Estimated uncertainties are represented by the error bars for a few points. The obtained dependencies are controlled by parameter χ which should be close to one to achieve the maximum enhancement effect. For the Maxwell-averaged rates the velocity in Eq. (1) should be replaced by the r.m.s. velocity $v_{\rm rms} = (3T/m)^{1/2}$. Therefore the rate peaks at the frequency which is proportional to the field amplitude and inversely proportional to the square root of temperature. In order to shift the optimal frequency to the near infrared region, we should either increase the field or decrease the temperature.

At lower temperatures the most favorable frequency for enhancement is in the range 0.003-0.005 a.u. (the wavelength in the range 9-15 μm), and the peak frequency increases

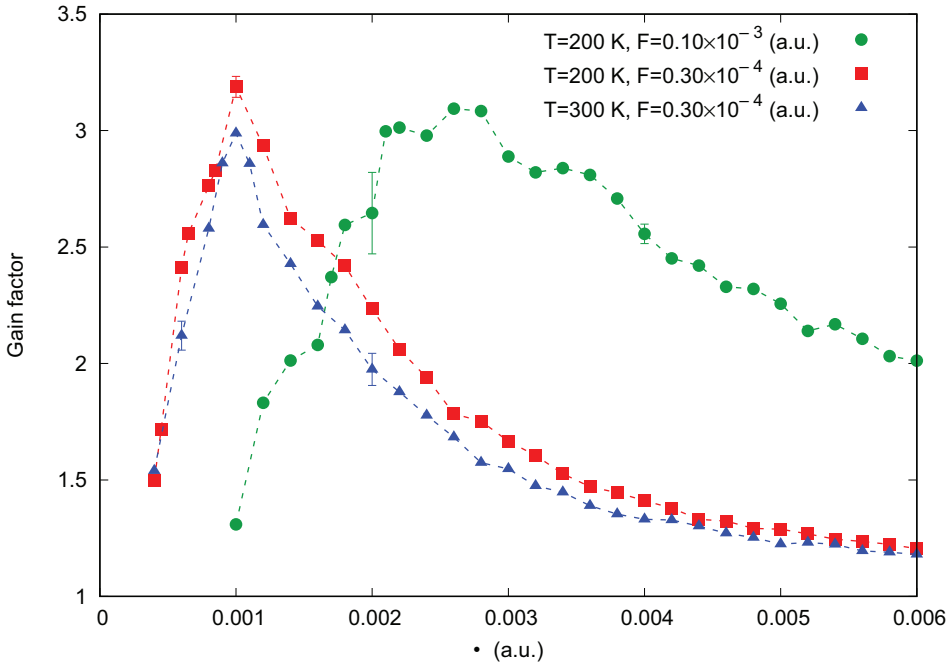

FIG. 6. The same as in Fig. 5 for higher temperatures.

with the increase of the field in accordance with the decrease of χ with the increase of F_0. As the temperature grows, so does the mean electron velocity, and the peak value of ω decreases further into far infrared, $\omega = 0.001$ a.u. (wavelength 45 μm). In general the gain factor is strongly suppressed due to the $\sin\theta_v$ factor in the integral (12), since the gain is the largest for $\theta_v = 0$ and π. Still, the gain factor can be substantial, about 2.5-3, for rather moderate fields in the range between 20 and 350 MW/cm^2.

IV. CONCLUSION AND OUTLOOK

The Coulomb focusing effect in LARR has been explored in the present paper for non-parallel geometries, that is for initial electron velocity nonparallel to the polarization of the laser field. The gain factor drops substantially with the increasing angle θ_v. The Maxwell-averaged rate constant for LARR is suppressed further because of the $\sin\theta_v$ factor in the phase space volume. However, even after all these reductions the gain factor can remain substantial, up to the factor 3, even for relatively moderate field of intensity 20 MW/cm^2. Field

frequencies used in the present work correspond to the far infrared radiation. However, it is possible to increase the frequency and achieve the same effect, if the field is increased as well, or the temperature/velocity is decreased, so that the χ parameter, Eq. (1) does not exceed 1. Our results might be important for various applications, particularly for antihydrogen formation in antiproton-positron plasma.

Although our studies are aimed at ultracold Maxwellian antihydrogen plasma, the present approach can be applied to other plasma conditions. First, it can be extended to plasmas formed by heavier elements. Provided that the atoms remain singly ionized, the bound electrons of larger elements would strongly influence the dynamics of LARR, and this will require a separate investigation. The assumption of Maxwellian distribution is relevant in the case of antihydrogen plasma [7, 8]. On the other hand large LARR cross sections in the low-energy region can deplete plasma of low-energy electrons (positrons) and lead to a non-Maxwellian distribution. There are other examples of non-Maxwellian cases, for example electron velocity distribution in storage ring experiments on RR [17–20]. These will also require separate studies.

ACKNOWLEDGMENTS

This work has been supported by the National Science Foundation, Grant No. PHY-2309261. HBA was supported by the US Department of Energy Office of Science, Basic Energy Sciences, under Grant No. DE-SC0021054.

APPENDIX A: THE TRANSFORMATION MATRIX

Using the coordinates of the basis vectors in the primed reference frame, Eqs. (6), (7), (8), we obtain the transformation matrix

$$\begin{pmatrix} \hat{x}\cdot\hat{x'} & \hat{x}\cdot\hat{y'} & \hat{x}\cdot\hat{z'} \\ \hat{y}\cdot\hat{x'} & \hat{y}\cdot\hat{y'} & \hat{y}\cdot\hat{z'} \\ \hat{z}\cdot\hat{x'} & \hat{z}\cdot\hat{y'} & \hat{z}\cdot\hat{z'} \end{pmatrix} = \begin{pmatrix} \cos\theta_v\cos\phi_v & -\sin\phi_v & \sin\theta_v\cos\phi_v \\ \cos\theta_v\sin\phi_v & \cos\phi_v & \sin\theta_v\sin\phi_v \\ -\sin\theta_v & 0 & \cos\theta_v \end{pmatrix}$$

Acting by this matrix on the column $\begin{pmatrix} b\cos\phi' \\ b\sin\phi' \\ -d \end{pmatrix}$, we arrive at the transformation (9), (10).

APPENDIX B: PLANAR TRAJECTORIES

The obvious case of a planar trajectory occurs when the initial velocity is parallel to the laser field polarization vector. We will discuss here a more nontrivial case when the impact parameter angle $\phi' = 0$, see Fig. 1. In this case, according to Eq. (9) the initial x and y coordinates are

$$x = \cos\phi_v(b\cos\theta_v - d\sin\theta_v), \qquad y = \sin\phi_v(b\cos\theta_v - d\sin\theta_v),$$

therefore $xv_y - yv_x = 0$, the component of the angular momentum along the laser field $L_z(0) = 0$, and $d\phi/dt = 0$. The variation of L_z at a later time is given by the Newton's equation

$$\frac{dL_z}{dt} = (\mathbf{r}\times\mathbf{F})_z$$

Since the Coulomb field is central, its contribution to the cross product is 0, and since the external field is directed along the z axis, its contribution to the z component to the cross product is 0 too, therefore $dL_z/dt = 0$, and $L_z = 0$ for all times. As a result $d\phi/dt = 0$ and the trajectory is planar. Generally L_z is a constant of the motion, but since $L_z \neq 0$, the trajectory is not planar.

[1] I. I. Fabrikant, H. B. Ambalampitiya, and I. F. Schneider, Phys. Rev. A **103**, 053115 (2021).

[2] H. B. Ambalampitiya, J. Stallbaumer, and I. I. Fabrikant, Phys. Rev. A **105**, 043111 (2022).

[3] K. Lévêque-Simon and P.-A. Hervieux, Phys. Rev. A **107**, 052813 (2023).

[4] P. B. Corkum, Phys. Rev. Lett. **71**, 1994 (1993).

[5] P. Agostini and L. F. DiMauro, Reports on Progress in Physics **67**, 813 (2004).

[6] P. B. Corkum and F. Krausz, Nature Physics **3**, 381 (2007).

[7] M. Charlton and D. P. V. D. Werf, Science Progress **98**, 34 (2015).

[8] W. A. Bertsche, E. Butler, M. Charlton, and N. Madsen, Journal of Physics B: Atomic, Molecular and Optical Physics **48**, 232001 (2015).

[9] M. H. Holzscheiter, M. Charlton, and M. M. Nieto, Physics Reports **402**, 1 (2004).

[10] G. Gabrielse, Advances in Atomic, Molecular and Optical Physics **50**, 155 (2005).

[11] F. Robicheaux, Journal of Physics B: Atomic, Molecular and Optical Physics **41**, 192001 (2008).

[12] M. Ahmadi *et al.*, Nature Communications **8**, 681 (2017).

[13] E. K. Anderson *et al.*, Nature **621**, 716 (2023).

[14] D. R. Bates, A. E. Kingston, and R. W. P. McWhirter, Proceedings of the Royal Society of London. Series A. Mathematical and Physical Sciences **267**, 297 (1962).

[15] H. B. Ambalampitiya and I. I. Fabrikant, Phys. Rev. A **99**, 063404 (2019).

[16] I. I. Fabrikant and H. B. Ambalampitiya, Phys. Rev. A **101**, 053401 (2020).

[17] R. Neumann, H. Poth, A. Winnacker, and A. Wolf, Zeitschrift für Physik A Atoms and Nuclei **313**, 253 (1983).

[18] U. Schramm, J. Berger, M. Grieser, D. Habs, E. Jaeschke, G. Kilgus, D. Schwalm, A. Wolf, R. Neumann, and R. Schuch, Phys. Rev. Lett. **67**, 22 (1991).

[19] A. Wolf, Hyperfine Interactions **76**, 189 (1993).

[20] A. Scrinzi, N. Elander, and A. Wolf, Zeitschrift für Physik D Atoms, Molecules and Clusters **34**, 185 (1995).

[21] A. Müller and A. Wolf, Hyperfine Interactions **109**, 233 (1997).

[22] M. L. Rogelstad, F. B. Yousif, T. J. Morgan, and J. B. A. Mitchell, Journal of Physics B: Atomic, Molecular and Optical Physics **30**, 3913 (1997).

[23] M. Amoretti *et al.* (ATHENA Collaboration), Phys. Rev. Lett. **97**, 213401 (2006).

[24] H. A. Kramers, The London, Edinburgh, and Dublin Philosophical Magazine and Journal of Science **46**, 836 (1923).

[25] L. D. Landau and E. M. Lifshitz, The Classical Theory of Fields, 3rd ed. (Pergamon, Oxford, 1971).

[26] M. Bell and J. S. Bell, Part. Accel. **12**, 49 (1982).

[27] V. Szebehely, Theory of Orbits: The Restricted Problem of Three Bodies (Academic Press, New York, 1967).

[28] H. Price, C. Lazarou, and A. Emmanouilidou, Phys. Rev. A **90**, 053419 (2014).

[29] G. P. Katsoulis, M. B. Peters, A. Staudte, R. Bhardwaj, and A. Emmanouilidou, Phys. Rev. A **103**, 033115 (2021).

[30] A. Emmanouilidou, M. B. Peters, and G. P. Katsoulis, Phys. Rev. A **107**, L041101 (2023).

[31] L. Wiesenfeld, Physics Letters A **144**, 467 (1990).

[32] L. Wiesenfeld, Acta Phys. Pol. B **23**, 271 (1992).

[33] L. Wiesenfeld, Journal of Physics B: Atomic, Molecular and Optical Physics **25**, 4373 (1992).